

GAS: Generative Avatar Synthesis from a Single Image

Yixing Lu¹ Junting Dong^{2†} Youngjoong Kwon³ Qin Zhao²
Bo Dai² Fernando De la Torre¹

¹Carnegie Mellon University ²Shanghai AI Laboratory ³Stanford University

Abstract

We introduce a generalizable and unified framework to synthesize view-consistent and temporally coherent avatars from a single image, addressing the challenging problem of single-image avatar generation. While recent methods employ diffusion models conditioned on human templates like depth or normal maps, they often struggle to preserve appearance information due to the discrepancy between sparse driving signals and the actual human subject, resulting in multi-view and temporal inconsistencies. Our approach bridges this gap by combining the reconstruction power of regression-based 3D human reconstruction with the generative capabilities of a diffusion model. The dense driving signal from the initial reconstructed human provides comprehensive conditioning, ensuring high-quality synthesis faithful to the reference appearance and structure. Additionally, we propose a unified framework that enables the generalization learned from novel pose synthesis on in-the-wild videos to naturally transfer to novel view synthesis. Our video-based diffusion model enhances disentangled synthesis with high-quality view-consistent renderings for novel views and realistic non-rigid deformations in novel pose animation. Results demonstrate the superior generalization ability of our method across in-domain and out-of-domain in-the-wild datasets. Project page: <https://humansensinglab.github.io/GAS/>

1. Introduction

Human avatar generation is a longstanding research area in computer vision and graphics, with applications spanning gaming, film, sports, fashion, and telepresence. Despite its potential to revolutionize daily life, current avatar generation technologies require costly capturing setups and highly complicated procedures, making them hard to access by broader audiences.

Recent efforts have sought to make avatar generation

more affordable by harnessing the power of neural rendering. In particular, some works [17, 21–23] focus on generalizable 3D human reconstruction that synthesize novel views and poses of arbitrary human subjects from very sparse or even single input images. These methods utilize 3D human priors to enable robust synthesis of complex human geometry, and interpolate well between available observations. However, due to their regression-based nature, they often struggle with extrapolation, leading to blurry results. In addition, they are often limited to rigid deformations.

Generative models like GANs and diffusion models have recently shown remarkable capability in producing photorealistic detailed images and videos with realistic dynamics. Building on the success of these generative techniques, several approaches use diffusion models conditioned on human priors (e.g., 2D keypoints, depth maps, or normal maps) to create high-quality avatars with realistic animation from a single image [6, 16, 41, 63]. However, due to the sparsity in these conditioning signals, the generated avatars often suffer from inconsistencies such as flickering across different views and over time.

To tackle these challenges, we propose a method for single-image avatar synthesis that achieves both view and temporal consistency. Instead of relying solely on sparse signals, we first generate intermediate novel views or poses using a regression-based 3D human reconstruction model. We then use them as conditioning inputs for a video diffusion model. By incorporating dense information from the 3D reconstruction, our approach preserves both structural accuracy and rich visual details, ensuring high-quality, consistent results across views and time.

Beyond selecting the appropriate driving signal, another key challenge is improving generalization to real-world data, because ultimately we want a system that works not just on controlled datasets but also on casually captured in-the-wild human images. Most human digitization models are trained on multi-view datasets captured in controlled studios [17, 21, 22], which lack the diversity of real-world scenarios, such as varied lighting, clothing, and motion. To address this, we propose to incorporate in-the-wild internet

[†] Corresponding author

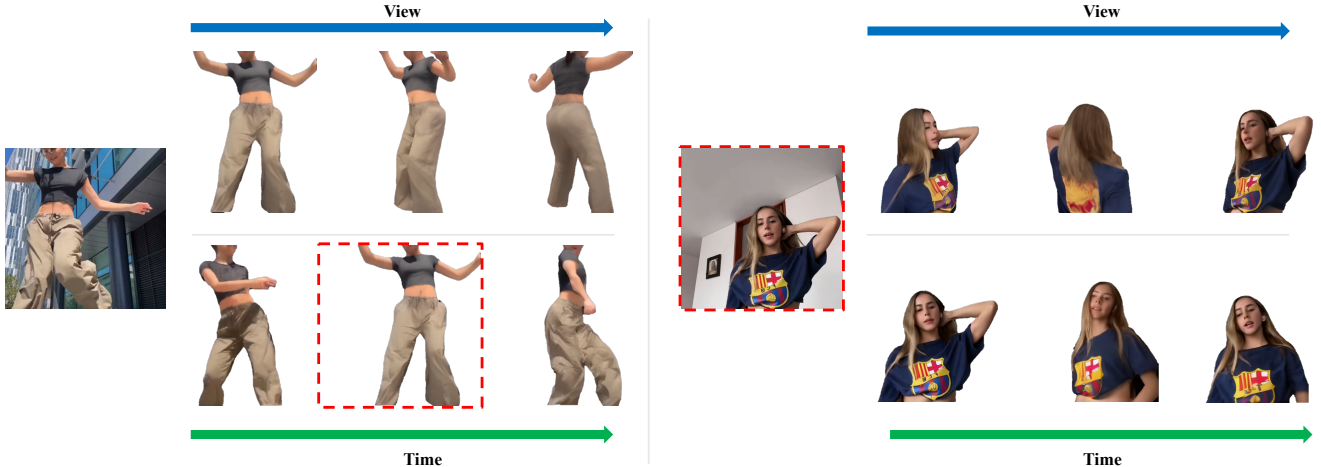


Figure 1. **In-the-wild avatar synthesis across views and time.** **Left:** The avatar is animated based on a pose sequence, enabling novel view generation from any chosen synthesized frame (highlighted by a red dashed rectangle). **Right:** Starting from a reference image (highlighted by a red dashed rectangle), we generate its novel views and animate the avatar through a given pose sequence.

videos, which provide an abundant source of diverse real-world distribution. While leveraging such videos significantly improves generalization, training a model on them presents challenges—particularly for novel view synthesis, which typically requires multi-view supervision, rarely available in internet videos.

To overcome this, we propose a unified framework that jointly learns novel view and pose synthesis, sharing parameters across tasks to enable cross-task generalization. While we still use studio multi-view datasets for novel view synthesis, we incorporate both multi-view and in-the-wild videos for novel pose synthesis. Since the same model parameters are used for both tasks, the generalization gained from pose synthesis naturally transfers to novel view synthesis as well. This approach significantly enhances the model’s ability to handle real-world data and improves overall synthesis quality as can be seen in Figure 1. Additionally, in order to employ this unified framework effectively, we introduce a mode switcher that differentiates between novel view and pose synthesis. This switcher disentangles the tasks, allowing the network to focus on view consistency when synthesizing novel views and realistic deformations when generating novel poses.

In summary, our main contributions are:

- A unified framework for novel view and pose synthesis of avatars, which enables shared model parameters across both tasks with real human data (e.g., internet videos) at scale for training, leading to broad generalizability.
- A dense appearance cue as synthesis guidance, ensuring consistent appearance preservation.
- A switcher integrated into the video diffusion model to enable disentangled modeling of static novel views and dynamic pose animation.

2. Related Work

2.1. Generalizable Human Radiance Fields

Radiance fields methods, like NeRF [31], have shown strong capabilities in generating high-fidelity renderings across views. To extend these methods to generalize to new scenes and handle sparse-view inputs, several approaches [40, 45, 54] have incorporated pixel-aligned features to aid novel view synthesis. However, applying these approaches directly to human modeling presents challenges due to the complex geometry of the human body, including self-occlusions, which often lead to overly smoothed outputs. To address these challenges, some methods [8, 9, 21, 22, 34, 35, 59] use 3D human templates, such as the SMPL model [30], to anchor features accurately on the human form. Although these techniques achieve good results even with sparse or single-view inputs [17], they are often hindered by slow rendering speeds. Recently, 3D Gaussian Splatting [20], optimized with GPU-based rasterization, has emerged as a promising radiance field representation, enabling faster rendering. Building on this, new methods [23, 62, 64] have achieved photorealistic human rendering from sparse observations. Nevertheless, these methods still struggle with producing clear details in unseen regions due to mean-seeking behavior in one-to-many mapping scenarios [24, 28]. In this work, we propose learning a distribution conditioned on generalizable human radiance fields, allowing us to synthesize clean, consistent view and pose sequences by sampling from this distribution.

2.2. Generative Human Animation

Generative human animation aims to employ generative models to produce coherent videos from static human im-

ages, utilizing guidance such as text and motion sequences. This body of work focuses on leveraging generative priors to sample complex dynamic motions, including pose-dependent clothing deformations. Early approaches harnessed the generative capabilities of Generative Adversarial Networks (GANs) [11] for synthesizing novel human poses [5, 27, 47]. In recent years, latent diffusion models [39] have gained traction in the realm of human animation due to their robust controllability and superior generation quality. Various methods [6, 7, 16, 25, 26, 42, 46, 63] implement distinct motion guidance and conditioning techniques. Notably, Animate Anyone [16] introduces a UNet-based ReferenceNet to extract features from reference images, utilizing DWPose [52] for pose guidance. Subsequent works [63] also incorporate guidance from 3D human parametric models, such as SMPL [30, 60, 61], leveraging the advantages of multiple forms of guidance. Following this trajectory, recent studies [14, 29, 36, 41] explore human view controllability within the diffusion frameworks. Human4DiT [41] develops a hierarchical 4D diffusion transformer that disentangles the learning of 2D images, viewpoints, and time. However, these methods struggle to synthesize view-consistent and temporally coherent results due to the gap between the sparse driving signal and the actual subject. In this paper, we propose a unified approach to human view and pose synthesis by conditioning on generalizable geometry and appearance features and mapping them to a cohesive representation, resulting in a more straightforward and effective process.

2.3. Diffusion Models for Video Generation

Diffusion models have demonstrated exceptional performance in image synthesis over the past few years. The research community has since started to extend these models to the more challenging task of video generation [56]. Significant efforts have been made to adapt UNet-based image diffusion models for video generation by incorporating additional temporal modules. Several studies [3, 12] have proposed freezing pre-trained image diffusion models and training only the newly added temporal module on video data. Stable Video Diffusion [2] adds temporal layers after each spatial convolution and attention layer, fine-tuning the entire model on large-scale, curated video datasets. It has proven to be a strong foundational model, facilitating further advancements in video generation as well as 3D/4D synthesis [44, 49]. Beyond UNet-based diffusion models, diffusion transformers [4, 33, 53] have emerged as a robust architecture for video generation, applying full attention to space-time patches of video and image latent codes. In this work, we opt to leverage the strong foundational capabilities of Stable Video Diffusion to model both multi-view correspondences and temporally coherent realistic deformations of human subjects.

3. Method

Our method generates view and time-wise coherent avatar renderings from a single image by leveraging the dense appearance information of a generalizable human reconstruction model combined with the generative capabilities of a video diffusion model.

3.1. Notation

Functions (e.g., neural network mapping) are denoted with uppercase calligraphic letters (e.g., \mathcal{U}). Vectors are denoted with bold lowercase letters (e.g., \mathbf{x}). Matrices are denoted with uppercase letters (e.g., C). Sets are denoted with bold uppercase letters (e.g., \mathcal{I}_{nerf}).

3.2. Single-view Generalizable Human Synthesis

Given a single reference image I_{ref} , the camera parameter P_{ref} , and the parameters of a human template, *i.e.*, the SMPL [30] model, we adopt single-view generalizable human NeRF [17] to synthesize an image corresponding to the target camera parameters P_{tar} and target template parameters consists of pose θ_{tar} and shape β_{tar} .

To render the target image, a point \mathbf{x} is sampled along the cast rays in the target space. Then it is transformed to point \mathbf{x}_e in the the SMPL canonical space via inverse LBS, where the features associated with \mathbf{x}_e are queried from the observation space. Specifically, pixel-aligned features and human template-conditioned features are obtained and fused together, denoted as \mathbf{p} . The density σ and color \mathbf{c} are obtained by a multi-layer perception (MLP) network \mathcal{F} :

$$\sigma(\mathbf{x}), \mathbf{c}(\mathbf{x}) = \mathcal{F}(\mathbf{x}, \mathbf{p}, \gamma_d(\mathbf{d})), \quad (1)$$

where γ_d is the positional encoding of viewing direction \mathbf{d} .

The target image I_{tar} in target view and pose is rendered using the volume rendering [31].

We emphasize that this human NeRF model is designed to generalize, enabling the synthesis of human appearances across a range of novel views and poses. However, due to its mean-seeking tendency, producing sharp renderings—particularly in occluded or unseen regions—remains challenging. This limitation motivates our introduction of generative priors to learn a distribution over the human views and poses, as discussed in the next section.

3.3. Synthesis as Video Generation Condition

In this section, we elaborate how we leverage video diffusion prior to reformulate the novel view and pose synthesis as a video generation task conditioned on the human radiance fields and human geometric templates. We would like to note that prior approaches often treat novel view and novel pose synthesis as separate tasks. In contrast, our approach unifies both tasks by conditioning on NeRF-rendered images, allowing for more consistent renderings.

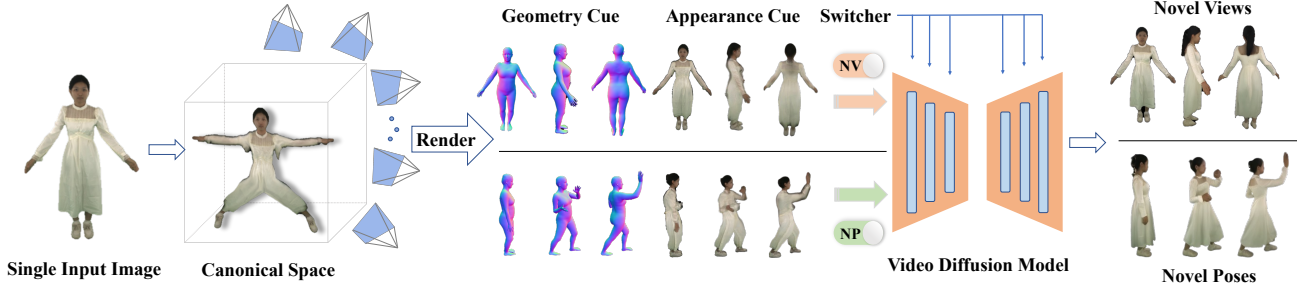


Figure 2. **Overview of our proposed method.** From a single input human image, our approach leverages a generalizable human NeRF to map the subject to canonical space, followed by reposing and rendering to obtain the appearance cue (*i.e.*, NeRF renderings). Paired with the geometry cue (*i.e.*, SMPL normal maps), they provide comprehensive conditions for the video diffusion model, enabling multi-view consistent novel view synthesis or temporally consistent pose animation, effectively disentangled by a switcher module.

Using human templates alone as a condition provides only sparse geometric guidance, which often leads to inconsistencies in appearance across novel views. By integrating generalizable radiance field as a unified conditioning mechanism, we address this issue and achieve better appearance consistency across varied poses and views.

Novel View Synthesis. Given a reference image I_{ref} and a camera trajectory $\{P_1, P_2, \dots, P_T\}$, we render the corresponding images $I_{nerf} = \{I_1, I_2, \dots, I_T\}$ from the NeRF, which serves as an input to our video diffusion model, *i.e.*, Stable Video Diffusion [2] that adopts spatio-temporal attention module and 3D residual convolution in the diffusion UNet. For the single input image I_{ref} , we extract its feature with CLIP [37] and repeat it for T times to match the number of frames, denoted as h_{clip} , which is then added to the video diffusion model through the cross attention. Meanwhile, we use the VAE encoder to encode our input image I_{ref} and obtain its latent feature C_{vae} .

To introduce NeRF renderings I_{nerf} to our video diffusion model, we feed I_{nerf} to the VAE encoder, after which it is further encoded by a small convolutional neural network. We denote the output latent feature as C_{nerf} .

In practice, we observe that solely relying on NeRF renderings in our video diffusion model is insufficient, as these renderings may sometimes exhibit artifacts, particularly due to inaccurate SMPL fittings or occlusions. Such artifacts can corrupt the guidance and hinder the diffusion model from learning meaningful conditional distributions. To address this limitation, we further integrate a geometric cue, *i.e.*, the SMPL model, to provide additional structural guidance. The SMPL model captures essential geometry information, which leads to the enhanced spatial consistency as well as the robust human shape recovery.

In order to integrate this information with the NeRF rendered features in the 2D pixel space, similar to [63], we render the human template mesh into 2D normal maps. Specifically, we render the SMPL normal maps $M = \{M_1, M_2, \dots, M_T\}$ under the camera trajectory $\{P_1, P_2, \dots, P_T\}$. Then a set of 2D convolution layers are

utilized to extract the features, denoted by C_{smpl} .

To effectively fuse C_{nerf} and C_{smpl} , we combine them through element-wise addition. The resulting fused feature is then added to the output of the first convolutional layer of the UNet in the video diffusion model.

Novel Pose Synthesis. Given a sequence of SMPL poses $\{\theta_1, \theta_2, \dots, \theta_T\}$ and a fixed camera parameter, we render corresponding images from the NeRF and SMPL normal maps. They can be used as conditions to the video diffusion model in the same manner as illustrated above.

Now we can formulate the learning objective of our diffusion model. The diffusion UNet \mathcal{U}_Θ predicts the noise ϵ for each diffusion step t , and our training objective is

$$\mathcal{L}_{\mathcal{U}_\Theta} = \mathbb{E} [\|\epsilon - \mathcal{U}_\Theta(Z_t, t, h_{clip}, C_{vae}, C_{nerf}, C_{smpl})\|] \quad (2)$$

where $Z_t = \alpha_t Z + \sigma_t \epsilon$. Here, Z is the ground-truth latent, $\epsilon \sim \mathcal{N}(0, I)$, and α_t and σ_t define the noise at timestep t . Θ is the learnable parameters of the UNet \mathcal{U} .

3.4. Switcher for Disentangled Synthesis

Joint learning of human view synthesis and pose synthesis presents inherent challenges for feed-forward methods. Our proposed framework addresses these challenges by unifying both tasks into a single video generation task, leveraging the capability of video diffusion model to effectively model each task under the same representation. Under this framework, a straightforward approach would be to train the video diffusion model on both multi-view and dynamic video data simultaneously. However, our empirical findings reveal that dynamic motions embedded within view synthesis videos can disrupt view consistency (see Figure 9). This issue arises due to the inherent modality differences between static view synthesis videos and dynamic animation videos. To mitigate this problem, we introduce a switcher mechanism within our video diffusion model that explicitly controls and disentangles these two modes, ensuring task-specific consistency and performance.

In particular, we introduce the switcher s , which is a one-hot vector that labels each of the two modalities, as the ad-

ditional condition to the video diffusion model. This allows us to extend the formulation in Equation 2 as follows:

$$\mathcal{L}_{U_\theta} = \mathbb{E} [\|\epsilon - \mathcal{U}_\theta(Z_t, t, \mathbf{h}_{\text{clip}}, C_{\text{vae}}, C_{\text{nerf}}, C_{\text{smpl}}, \mathbf{s})\|] \quad (3)$$

To incorporate the domain switcher \mathbf{s} , we first apply positional encoding and then concatenate it with the time embedding. This combined encoding is subsequently fed into the UNet within the video diffusion model.

3.5. Training and Inference

Training. The entire training process of our pipeline consists of two stages. During the first stage, we train the generalizable human NeRF \mathcal{F} model on the multi-view datasets. Following [17], we randomly sample observation and target image pairs from each subject. The prediction of the target view is supervised by minimizing the loss objective $\mathcal{L} = \mathcal{L}_2 + \lambda_{\text{ssim}} \cdot \mathcal{L}_{\text{ssim}} + \lambda_{\text{lpiips}} \cdot \mathcal{L}_{\text{lpiips}} + \lambda_{\text{mask}} \cdot \mathcal{L}_{\text{mask}}$ where $\mathcal{L}_2, \mathcal{L}_{\text{ssim}}, \mathcal{L}_{\text{lpiips}}$ are photometric L_2 loss, SSIM loss [48] and LPIPS [57] loss between the predicted image and the ground truth. $\mathcal{L}_{\text{mask}}$ is the L_2 difference between the accumulated volume density and the ground truth human binary mask. $\lambda_{\text{ssim}}, \lambda_{\text{lpiips}}, \lambda_{\text{mask}}$ are weights of each loss to balance their contributions to the final loss function.

In the second stage, we freeze the generalizable NeRF model and train our video diffusion model. We train the full spatio-temporal UNet and feature encoders for NeRF and SMPL normal renderings following our training objective in Equation 3. The second stage is trained on our complete dataset to ensure the generalization.

Inference. We apply classifier-free guidance (CFG) [15] to inference from the video diffusion model. The two tasks are done with different CFG schedules according to the task properties. For the novel view synthesis task, we utilize a triangular CFG scaling [44], where we linearly increase CFG from 1 at the front view to 2 at the back view, then linearly decrease it back to 1 at the front view. For the novel pose synthesis task, we fix the CFG scale to be 2.

4. Experiments

4.1. Experimental Setup

4.1.1. Datasets

3D Scans. We use THuman2.1 [55] and 2K2K dataset [13] with around 4500 3D scans in total. THuman2.1 comprises 2445 high-quality 3D scans and texture maps. We randomly sample 2345 subjects for training and the remaining 100 subjects for testing. 2K2K dataset consists of 2000 train and 50 test subjects, totally 2050 scans. For both datasets, RGB images are rendered from 20 uniformly distributed views around the scan, at the resolution of 1024×1024 . SMPL parameters are estimated using off-the-shelf method for multi-view SMPL fitting [1].

Multi-view Videos. MVHumanNet [50] is a multi-view video dataset featuring a large number of diverse identities and everyday clothing. We use a subset of 944 human captures, each consisting of synchronized 16-view videos per subject. We reserve 48 subjects for evaluation and use the remaining subjects for training. The dataset also includes SMPL parameters, optimized from multi-view images.

Monocular Videos. For in-the-wild datasets, we use the TikTok dataset [19] and an additional collection of internet videos. The TikTok dataset includes 350 dance videos, from which we processed and filtered 289 valid video sequences for training. Following the protocol in [6, 46], we use subjects from 335 to 340 for testing. To further diversify the data, we selected 122 video sequences from Champ [63] training dataset, originally sourced from reputable online platforms such as TikTok and YouTube. For both datasets, we obtain the foreground human masks using Grounded-SAM [38] and the SMPL parameters using 4DHumans [10].

4.1.2. Implementation Details

We trained the generalizable human NeRF model [17] on MVHumanNet dataset. To accelerate the video diffusion training, instead of creating and rendering the human NeRF on-the-fly, we choose to store the NeRF renderings for all datasets offline. For the video diffusion model, we initialize it with the pre-trained Stable Video Diffusion 1.1 image-to-video model ¹ [2]. We resize all images to a resolution of 512×512 . Each batch consists of 20 frames. We train the model for 150k iterations with an effective batch size of 8 and a learning rate of 10^{-5} . We utilize 8 A100 GPUs and the total training time is 3 days.

4.1.3. Baselines and Metrics

Baselines. We benchmark our method against state-of-the-art generative human rendering methods including Champ [63] and Animate Anyone [16]. As for Animate Anyone [16], we use the implementations from Moore Threads ².

Metrics. We evaluate the fidelity and consistency of our results using both image-level and video-level metrics. For image-level comparisons, we report peak signal-to-noise ratio (PSNR), structural similarity index measure (SSIM) [48], and learned perceptual image patch similarity (LPIPS) [57]. For video-level evaluation, we use the Fréchet Video Distance (FVD) [43] metric.

4.2. Comparisons on Novel View Synthesis

We show the comparisons with Animate Anyone [16] and Champ [63], which are two competitors focusing on generative human synthesis. For a fair comparison, we fine-tuned both methods on our full 3D scan dataset for 10k iterations.

¹<https://huggingface.co/stabilityai/stable-video-diffusion-img2vid-xt-1-1>

²<https://github.com/MooreThreads/Moore-AnimateAnyone>

Method	PSNR \uparrow		SSIM \uparrow		LPIPS \downarrow		FVD \downarrow	
	THuman	2K2K	THuman	2K2K	THuman	2K2K	THuman	2K2K
Animate Anyone	22.48	18.48	0.927	0.557	0.061	0.263	460.3	1422.1
Champ	20.96	22.14	0.909	0.910	0.074	0.075	470.3	480.3
Animate Anyone*	25.20	26.22	0.938	0.936	0.046	0.050	302.7	286.4
Champ*	23.89	25.66	0.928	0.935	0.054	0.052	296.1	279.3
Ours	26.77	28.82	0.943	0.954	0.041	0.039	194.8	191.3

Table 1. **Quantitative comparison for novel view synthesis on THuman and 2K2K dataset.** For all the methods, we report the average score on 20 views using four orthogonal input views (front, back, and side views). * indicates methods fine-tuned on our 3D scan dataset.



Figure 3. **Qualitative comparisons for novel view synthesis on THuman dataset.** Inconsistent areas across views are marked with red circles, e.g., the hair regions are inconsistent between frontal and back views. * denotes a method fine-tuned on our full 3D scan dataset.

Quantitative results. We adopt a comprehensive evaluation protocol for human novel view synthesis from a single image. Specifically, for each subject, we sample four orthogonal input views and compute their mean score across all generated novel views. It is worth noting that Animate

Anyone [16] often produces a noisy background. For a fair comparison that focuses solely on the human subjects, we apply the ground truth mask to remove backgrounds in the THuman dataset, while in the 2K2K dataset, we retain the generated images as they are.

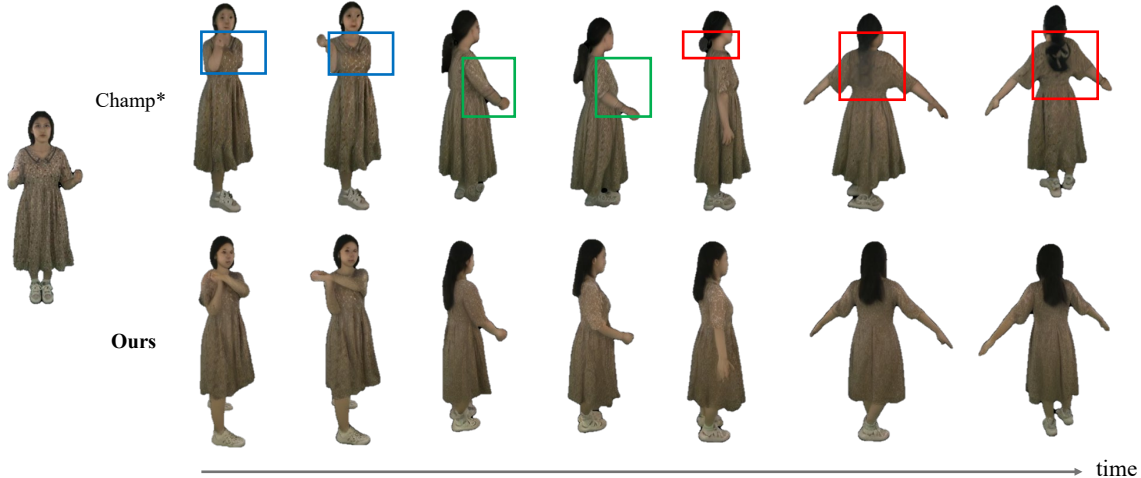


Figure 4. **Qualitative comparisons for novel pose synthesis on MVHumanNet.** In the first row of Champ [63] results, blue rectangles mark disappearing arms, green rectangles show varying sleeve lengths, and red rectangles indicate inconsistencies in hair appearance. * denotes a method further fine-tuned using our complete animation video dataset.

Quantitative results are presented in Table 1. Results show that our method achieves state-of-the-art performance across all evaluation metrics, highlighting the advantages of our generalizable human radiance field in preserving intricate details across viewpoint changes.

Qualitative results. Figure 3 presents our qualitative comparisons with baseline methods, focusing on challenging reference views and novel views that have less overlapping.

4.3. Comparisons on Novel Pose Synthesis

We compare our method on novel pose synthesis task with strong baseline methods Animate Anyone [16] and Champ [63], which are designed for single-image animation. For a fair comparison, we also further fine-tuned the baseline methods on our complete video dataset for 10k iterations.

Quantitative results. To evaluate on the TikTok dataset, we randomly sample a frame as the reference and generate the subsequent 100 frames. Quantitative results are presented in Table 2. Our method consistently outperforms the baseline methods, even after additional fine-tuning.

Qualitative results. Qualitative results are shown in Figure 4, where we compare our method with Champ [63] on the novel view animation task for the MVHumanNet dataset. Competing methods display flickering and fluctuations, especially in unseen regions. In contrast, ours synthesizes temporally consistent animations, even from novel views.

4.4. Ablation Studies and Analyses

We conduct ablation studies evaluating variants of our proposed method. Please refer to the supplement for more ablations with quantitative and qualitative comparisons.

Method	PSNR \uparrow	SSIM \uparrow	LPIPS \downarrow	FVD \downarrow
Animate Anyone	17.21	0.762	0.225	1274.1
Champ	18.48	0.806	0.182	585.0
Animate Anyone*	17.83	0.791	0.204	840.5
Champ*	18.57	0.797	0.187	893.7
Ours	19.11	0.833	0.176	362.0

Table 2. **Quantitative comparisons for novel pose synthesis on TikTok dataset.** * Indicates methods fine-tuned on our multi-view video and monocular video dataset.

Generalizable geometry and appearance cues. To study the effect of both geometry (*i.e.*, SMPL normal map) and appearance cues (*i.e.*, human radiance field), we train a variant with the geometry cue completely removed and a variant with appearance cue removed. Our hypothesis for the generalizable human radiance field is that it provides rich and consistent appearance cues across different views and times. To validate this, we present quantitative comparisons for novel view synthesis on the THuman dataset and pose animation from a novel view on the MVHumanNet dataset. As shown in Table 3, our approach consistently improved performance across both tasks and datasets.

Metric: FVD \downarrow	THuman	MVHumanNet
w.o. appear. cue	207.5	234.6
w. appear. cue	194.8	188.5

Table 3. **Quantitative ablation study on our appearance cue.** Please refer to Table 10 in the supplement for a complete quantitative evaluation on geometry and appearance cues.

To demonstrate the importance of the geometry cue, we present a qualitative ablation study on internet videos (*e.g.*,

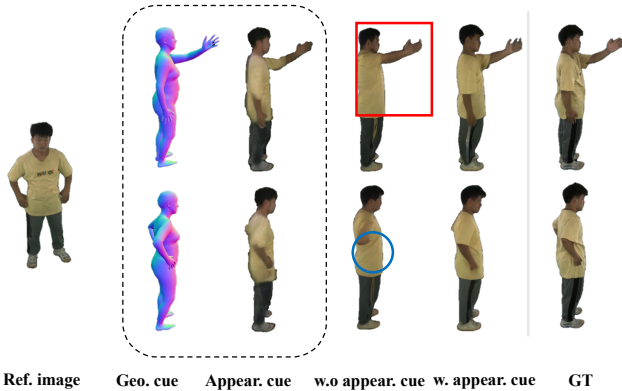


Figure 5. **Ablation study on the appearance cue.** Without the appearance cue, artifacts include incorrect arm raises (red rectangles) and distorted hand placement on the waist (blue circles), both resolved with the appearance cue.

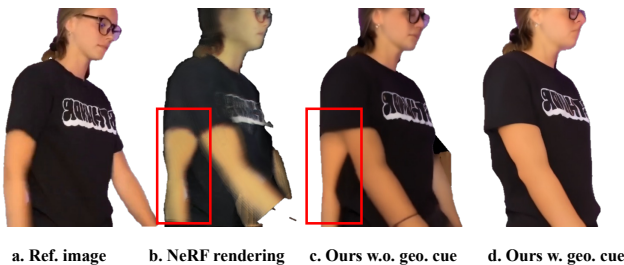


Figure 6. **Ablation study on the geometry cue.** Without the geometry cue, occlusion leads human NeRF to misinterpret the arm as clothing texture, which further misleads diffusion generation (red rectangles).



Figure 7. **Novel view synthesis on real-world human subjects.**

TikTok dataset). Occlusion is a common challenge in in-the-wild videos, often causing artifacts in generalizable human radiance fields due to pixel-aligned feature extraction and warping. As shown in Figure 6, without a clean geometry guidance, the radiance field can misguide the diffusion generation, leading to visible distortions.

Mixed training with 3D/multi-view captures and internet videos. We analyze the impact of our training strategy,



Figure 8. **Ablation on involving internet videos for training.**

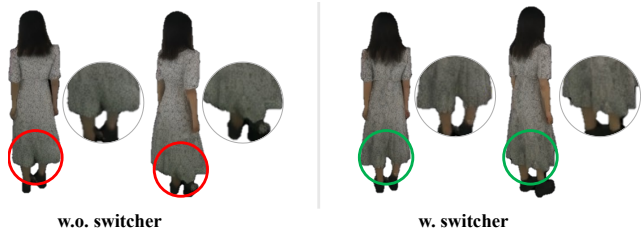


Figure 9. **Ablation on the switcher for disentangling static view and dynamic motion synthesis.** Without the switcher, undesired clothing deformations—such as dress swinging—are involved in the static novel view generation.

which leverages diverse data sources, aiming to improve generalizability. As shown in Figure 7, our model demonstrates strong generalization capability for novel view synthesis in real-world scenarios. Figure 8 presents an ablation on involving internet videos for training.

Effect of switcher for disentangled synthesis. In our setup, where we jointly learn static view synthesis and dynamic motion modeling, we introduce a switcher module. To illustrate the effectiveness of this switcher, we train a model variant without the switcher and present qualitative ablation studies. Without the switcher, dynamic motion often appears in the generated consecutive novel views, as shown in Figure 9.

5. Conclusion

We present a generalizable and unified framework for avatar synthesis from a single image, addressing key challenges in appearance consistency and generalization to in-the-wild avatars. Our approach integrates a regression-based human radiance field with a video diffusion model, effectively utilizing dense conditioning to minimize discrepancies between driving signals and target representations. Additionally, our framework enables large-scale training on realistic human data from different sources, while maintaining a disentangled modeling of static novel views and dynamic motion. This synergy leads to high-fidelity view synthesis and pose animation with lifelike deformations, demonstrating strong generalization across diverse real-world scenarios.

References

- [1] Easymocap - make human motion capture easier. Github, 2021. 5
- [2] Andreas Blattmann, Tim Dockhorn, Sumith Kulal, Daniel Mendelevitch, Maciej Kilian, Dominik Lorenz, Yam Levi, Zion English, Vikram Voleti, Adam Letts, et al. Stable video diffusion: Scaling latent video diffusion models to large datasets. *arXiv preprint arXiv:2311.15127*, 2023. 3, 4, 5, 12
- [3] Andreas Blattmann, Robin Rombach, Huan Ling, Tim Dockhorn, Seung Wook Kim, Sanja Fidler, and Karsten Kreis. Align your latents: High-resolution video synthesis with latent diffusion models. In *Proceedings of the IEEE/CVF Conference on Computer Vision and Pattern Recognition*, pages 22563–22575, 2023. 3
- [4] Tim Brooks, Bill Peebles, Connor Holmes, Will DePue, Yufei Guo, Li Jing, David Schnurr, Joe Taylor, Troy Luhman, Eric Luhman, Clarence Ng, Ricky Wang, and Aditya Ramesh. Video generation models as world simulators. 2024. 3
- [5] Caroline Chan, Shiry Ginosar, Tinghui Zhou, and Alexei A Efros. Everybody dance now. In *IEEE International Conference on Computer Vision (ICCV)*, 2019. 3
- [6] Di Chang, Yichun Shi, Quankai Gao, Hongyi Xu, Jessica Fu, Guoxian Song, Qing Yan, Yizhe Zhu, Xiao Yang, and Mohammad Soleymani. Magicpose: Realistic human poses and facial expressions retargeting with identity-aware diffusion. In *Forty-first International Conference on Machine Learning*, 2023. 1, 3, 5, 12
- [7] Di Chang, Hongyi Xu, You Xie, Yipeng Gao, Zhengfei Kuang, Shengqu Cai, Chenxu Zhang, Guoxian Song, Chao Wang, Yichun Shi, et al. X-dyna: Expressive dynamic human image animation. *arXiv preprint arXiv:2501.10021*, 2025. 3
- [8] Junting Dong, Qi Fang, Yudong Guo, Sida Peng, Qing Shuai, Xiaowei Zhou, and Hujun Bao. Totalselfscan: Learning full-body avatars from self-portrait videos of faces, hands, and bodies. In *Advances in Neural Information Processing Systems*, 2022. 2
- [9] Junting Dong, Qi Fang, Tianshuo Yang, Qing Shuai, Chengyu Qiao, and Sida Peng. ivs-net: Learning human view synthesis from internet videos. In *Proceedings of the IEEE/CVF International Conference on Computer Vision*, pages 22942–22951, 2023. 2
- [10] Shubham Goel, Georgios Pavlakos, Jathushan Rajasegaran, Angjoo Kanazawa, and Jitendra Malik. Humans in 4D: Reconstructing and tracking humans with transformers. In *ICCV*, 2023. 5
- [11] Ian Goodfellow, Jean Pouget-Abadie, Mehdi Mirza, Bing Xu, David Warde-Farley, Sherjil Ozair, Aaron Courville, and Yoshua Bengio. Generative adversarial nets. *Advances in neural information processing systems*, 27, 2014. 3
- [12] Yuwei Guo, Ceyuan Yang, Anyi Rao, Zhengyang Liang, Yaohui Wang, Yu Qiao, Maneesh Agrawala, Dahua Lin, and Bo Dai. Animatediff: Animate your personalized text-to-image diffusion models without specific tuning. *arXiv preprint arXiv:2307.04725*, 2023. 3, 15
- [13] Sang-Hun Han, Min-Gyu Park, Ju Hong Yoon, Ju-Mi Kang, Young-Jae Park, and Hae-Gon Jeon. High-fidelity 3d human digitization from single 2k resolution images. In *IEEE Conference on Computer Vision and Pattern Recognition (CVPR2023)*, 2023. 5, 12
- [14] Xu He, Xiaoyu Li, Di Kang, Jiangnan Ye, Chaopeng Zhang, Liyang Chen, Xiangjun Gao, Han Zhang, Zhiyong Wu, and Haolin Zhuang. Magicman: Generative novel view synthesis of humans with 3d-aware diffusion and iterative refinement. *arXiv preprint arXiv:2408.14211*, 2024. 3
- [15] Jonathan Ho and Tim Salimans. Classifier-free diffusion guidance. *arXiv preprint arXiv:2207.12598*, 2022. 5
- [16] Li Hu, Xin Gao, Peng Zhang, Ke Sun, Bang Zhang, and Liefeng Bo. Animate anyone: Consistent and controllable image-to-video synthesis for character animation. *arXiv preprint arXiv:2311.17117*, 2023. 1, 3, 5, 6, 7, 13, 15
- [17] Shoukang Hu, Fangzhou Hong, Liang Pan, Haiyi Mei, Lei Yang, and Ziwei Liu. Sherf: Generalizable human nerf from a single image. In *Proceedings of the IEEE/CVF International Conference on Computer Vision*, pages 9352–9364, 2023. 1, 2, 3, 5
- [18] Zehuan Huang, Hao Wen, Junting Dong, Yaohui Wang, Yanguang Li, Xinyuan Chen, Yan-Pei Cao, Ding Liang, Yu Qiao, Bo Dai, et al. Epidiff: Enhancing multi-view synthesis via localized epipolar-constrained diffusion. In *Proceedings of the IEEE/CVF Conference on Computer Vision and Pattern Recognition*, pages 9784–9794, 2024. 15
- [19] Yasamin Jafarian and Hyun Soo Park. Learning high fidelity depths of dressed humans by watching social media dance videos. In *Proceedings of the IEEE/CVF Conference on Computer Vision and Pattern Recognition*, pages 12753–12762, 2021. 5, 12, 13
- [20] Bernhard Kerbl, Georgios Kopanas, Thomas Leimkühler, and George Drettakis. 3d gaussian splatting for real-time radiance field rendering. *ACM Trans. Graph.*, 42(4):139–1, 2023. 2
- [21] Youngjoong Kwon, Dahun Kim, Duygu Ceylan, and Henry Fuchs. Neural human performer: Learning generalizable radiance fields for human performance rendering. *Advances in Neural Information Processing Systems*, 34:24741–24752, 2021. 1, 2
- [22] Youngjoong Kwon, Dahun Kim, Duygu Ceylan, and Henry Fuchs. Neural image-based avatars: Generalizable radiance fields for human avatar modeling. *arXiv preprint arXiv:2304.04897*, 2023. 1, 2
- [23] Youngjoong Kwon, Baole Fang, Yixing Lu, Haoye Dong, Cheng Zhang, Francisco Vicente Carrasco, Albert Mosella-Montoro, Jianjin Xu, Shingo Takagi, Daeil Kim, et al. Generalizable human gaussians for sparse view synthesis. *arXiv preprint arXiv:2407.12777*, 2024. 1, 2
- [24] Youngjoong Kwon, Lingjie Liu, Henry Fuchs, Marc Habermann, and Christian Theobalt. Deliffas: Deformable light fields for fast avatar synthesis. *Advances in Neural Information Processing Systems*, 36, 2024. 2
- [25] Boyi Li, Jathushan Rajasegaran, Yossi Gandelsman, Alexei A Efros, and Jitendra Malik. Synthesizing moving people with 3d control. *arXiv preprint arXiv:2401.10889*, 2024. 3

- [26] Hongxiang Li, Yaowei Li, Yuhang Yang, Junjie Cao, Zhihong Zhu, Xuxin Cheng, and Long Chen. Dispose: Disentangling pose guidance for controllable human image animation. *arXiv preprint arXiv:2412.09349*, 2024. 3
- [27] Lingjie Liu, Weipeng Xu, Michael Zollhoefer, Hyeonwoo Kim, Florian Bernard, Marc Habermann, Wenping Wang, and Christian Theobalt. Neural rendering and reenactment of human actor videos. *ACM Transactions on Graphics (TOG)*, 38(5):1–14, 2019. 3
- [28] Lingjie Liu, Marc Habermann, Viktor Rudnev, Kripasindhu Sarkar, Jiatao Gu, and Christian Theobalt. Neural actor: Neural free-view synthesis of human actors with pose control. *ACM transactions on graphics (TOG)*, 40(6):1–16, 2021. 2
- [29] Zhibin Liu, Haoye Dong, Aviral Chharia, and Hefeng Wu. Human-vdm: Learning single-image 3d human gaussian splatting from video diffusion models. *arXiv preprint arXiv:2409.02851*, 2024. 3
- [30] Matthew Loper, Naureen Mahmood, Javier Romero, Gerard Pons-Moll, and Michael J Black. Smpl: a skinned multi-person linear model. *ACM Transactions on Graphics (TOG)*, 34(6):1–16, 2015. 2, 3, 12
- [31] Ben Mildenhall, Pratul P Srinivasan, Matthew Tancik, Jonathan T Barron, Ravi Ramamoorthi, and Ren Ng. Nerf: Representing scenes as neural radiance fields for view synthesis. *Communications of the ACM*, 65(1):99–106, 2021. 2, 3
- [32] Panwang Pan, Zhuo Su, Chenguo Lin, Zhen Fan, Yongjie Zhang, Zeming Li, Tingting Shen, Yadong Mu, and Yebin Liu. Humansplat: Generalizable single-image human gaussian splatting with structure priors. *arXiv preprint arXiv:2406.12459*, 2024. 15
- [33] William Peebles and Saining Xie. Scalable diffusion models with transformers. In *Proceedings of the IEEE/CVF International Conference on Computer Vision*, pages 4195–4205, 2023. 3, 12
- [34] Sida Peng, Junting Dong, Qianqian Wang, Shangzhan Zhang, Qing Shuai, Xiaowei Zhou, and Hujun Bao. Animatable neural radiance fields for modeling dynamic human bodies. In *ICCV*, 2021. 2
- [35] Sida Peng, Yuanqing Zhang, Yinghao Xu, Qianqian Wang, Qing Shuai, Hujun Bao, and Xiaowei Zhou. Neural body: Implicit neural representations with structured latent codes for novel view synthesis of dynamic humans. In *CVPR*, 2021. 2
- [36] Lingteng Qiu, Shenhao Zhu, Qi Zuo, Xiaodong Gu, Yuan Dong, Junfei Zhang, Chao Xu, Zhe Li, Weihao Yuan, Liefeng Bo, et al. Anigs: Animatable gaussian avatar from a single image with inconsistent gaussian reconstruction. *arXiv preprint arXiv:2412.02684*, 2024. 3
- [37] Alec Radford, Jong Wook Kim, Chris Hallacy, Aditya Ramesh, Gabriel Goh, Sandhini Agarwal, Girish Sastry, Amanda Askell, Pamela Mishkin, Jack Clark, et al. Learning transferable visual models from natural language supervision. In *International conference on machine learning*, pages 8748–8763. PMLR, 2021. 4
- [38] Tianhe Ren, Shilong Liu, Ailing Zeng, Jing Lin, Kunchang Li, He Cao, Jiayu Chen, Xinyu Huang, Yukang Chen, Feng Yan, Zhaoyang Zeng, Hao Zhang, Feng Li, Jie Yang, Hongyang Li, Qing Jiang, and Lei Zhang. Grounded sam: Assembling open-world models for diverse visual tasks, 2024. 5
- [39] Robin Rombach, Andreas Blattmann, Dominik Lorenz, Patrick Esser, and Björn Ommer. High-resolution image synthesis with latent diffusion models. In *Proceedings of the IEEE/CVF conference on computer vision and pattern recognition*, pages 10684–10695, 2022. 3
- [40] Shunsuke Saito, Zeng Huang, Ryota Natsume, Shigeo Morishima, Angjoo Kanazawa, and Hao Li. Pifu: Pixel-aligned implicit function for high-resolution clothed human digitization. In *Proceedings of the IEEE/CVF international conference on computer vision*, pages 2304–2314, 2019. 2
- [41] Ruizhi Shao, Youxin Pang, Zerong Zheng, Jingxiang Sun, and Yebin Liu. Human4dit: Free-view human video generation with 4d diffusion transformer. *arXiv preprint arXiv:2405.17405*, 2024. 1, 3, 14
- [42] Mingze Sun, Junhao Chen, Junting Dong, Yurun Chen, Xinyu Jiang, Shiwei Mao, Puhua Jiang, Jingbo Wang, Bo Dai, and Ruqi Huang. Drive: Diffusion-based rigging empowers generation of versatile and expressive characters. *arXiv preprint arXiv:2411.17423*, 2024. 3
- [43] Thomas Unterthiner, Sjoerd Van Steenkiste, Karol Kurach, Raphael Marinier, Marcin Michalski, and Sylvain Gelly. Towards accurate generative models of video: A new metric & challenges. *arXiv preprint arXiv:1812.01717*, 2018. 5
- [44] Vikram Voleti, Chun-Han Yao, Mark Boss, Adam Letts, David Pankratz, Dmitrii Tochilkin, Christian Laforte, Robin Rombach, and Varun Jampani. SV3D: Novel multi-view synthesis and 3D generation from a single image using latent video diffusion. In *European Conference on Computer Vision (ECCV)*, 2024. 3, 5
- [45] Peihao Wang, Xuxi Chen, Tianlong Chen, Subhashini Venugopalan, Zhangyang Wang, et al. Is attention all that nerf needs? *arXiv preprint arXiv:2207.13298*, 2022. 2
- [46] Tan Wang, Linjie Li, Kevin Lin, Yuanhao Zhai, Chung-Ching Lin, Zhengyuan Yang, Hanwang Zhang, Zicheng Liu, and Lijuan Wang. Disco: Disentangled control for realistic human dance generation. In *Proceedings of the IEEE/CVF Conference on Computer Vision and Pattern Recognition*, pages 9326–9336, 2024. 3, 5
- [47] Ting-Chun Wang, Arun Mallya, and Ming-Yu Liu. One-shot free-view neural talking-head synthesis for video conferencing. In *Proceedings of the IEEE/CVF conference on computer vision and pattern recognition*, pages 10039–10049, 2021. 3
- [48] Zhou Wang, Alan C Bovik, Hamid R Sheikh, and Eero P Simoncelli. Image quality assessment: from error visibility to structural similarity. *IEEE transactions on image processing*, 13(4):600–612, 2004. 5
- [49] Yiming Xie, Chun-Han Yao, Vikram Voleti, Huaizu Jiang, and Varun Jampani. SV4D: Dynamic 3d content generation with multi-frame and multi-view consistency. *arXiv preprint arXiv:2407.17470*, 2024. 3
- [50] Zhangyang Xiong, Chenghong Li, Kenkun Liu, Hongjie Liao, Jianqiao Hu, Junyi Zhu, Shuliang Ning, Lingteng Qiu,

- Chongjie Wang, Shijie Wang, et al. Mvhumannet: A large-scale dataset of multi-view daily dressing human captures. In *Proceedings of the IEEE/CVF Conference on Computer Vision and Pattern Recognition*, pages 19801–19811, 2024. 5, 12, 13, 14, 15, 16
- [51] Zhongcong Xu, Chaoyue Song, Guoxian Song, Jianfeng Zhang, Jun Hao Liew, Hongyi Xu, You Xie, Linjie Luo, Guosheng Lin, Jiashi Feng, et al. High quality human image animation using regional supervision and motion blur condition. *arXiv preprint arXiv:2409.19580*, 2024. 12
- [52] Zhendong Yang, Ailing Zeng, Chun Yuan, and Yu Li. Effective whole-body pose estimation with two-stages distillation. In *Proceedings of the IEEE/CVF International Conference on Computer Vision*, pages 4210–4220, 2023. 3
- [53] Zhuoyi Yang, Jiayan Teng, Wendi Zheng, Ming Ding, Shiyu Huang, Jiazheng Xu, Yuanming Yang, Wenyi Hong, Xiaohan Zhang, Guanyu Feng, et al. Cogvideox: Text-to-video diffusion models with an expert transformer. *arXiv preprint arXiv:2408.06072*, 2024. 3, 12
- [54] Alex Yu, Vickie Ye, Matthew Tancik, and Angjoo Kanazawa. pixelnerf: Neural radiance fields from one or few images. In *Proceedings of the IEEE/CVF conference on computer vision and pattern recognition*, pages 4578–4587, 2021. 2
- [55] Tao Yu, Zerong Zheng, Kaiwen Guo, Pengpeng Liu, Qionghai Dai, and Yebin Liu. Function4d: Real-time human volumetric capture from very sparse consumer rgbd sensors. In *IEEE Conference on Computer Vision and Pattern Recognition (CVPR2021)*, 2021. 5, 12, 13, 14
- [56] Ailing Zeng, Yuhang Yang, Weidong Chen, and Wei Liu. The dawn of video generation: Preliminary explorations with sora-like models. *arXiv preprint arXiv:2410.05227*, 2024. 3
- [57] Richard Zhang, Phillip Isola, Alexei A Efros, Eli Shechtman, and Oliver Wang. The unreasonable effectiveness of deep features as a perceptual metric. In *Proceedings of the IEEE conference on computer vision and pattern recognition*, pages 586–595, 2018. 5
- [58] Yuang Zhang, Jiayi Gu, Li-Wen Wang, Han Wang, Junqi Cheng, Yuefeng Zhu, and Fangyuan Zou. Mimicmotion: High-quality human motion video generation with confidence-aware pose guidance. *arXiv preprint arXiv:2406.19680*, 2024. 12, 14
- [59] Fuqiang Zhao, Wei Yang, Jiakai Zhang, Pei Lin, Yingliang Zhang, Jingyi Yu, and Lan Xu. Humannerf: Efficiently generated human radiance field from sparse inputs. In *Proceedings of the IEEE/CVF Conference on Computer Vision and Pattern Recognition (CVPR)*, pages 7743–7753, 2022. 2
- [60] Yizhou Zhao, Hengwei Bian, Kaihua Chen, Pengliang Ji, Liao Qu, Shao-yu Lin, Weichen Yu, Haoran Li, Hao Chen, Jun Shen, et al. Metric from human: Zero-shot monocular metric depth estimation via test-time adaptation. In *The Thirty-eighth Annual Conference on Neural Information Processing Systems*, 2024. 3
- [61] Yizhou Zhao, Tuanfeng Yang Wang, Bhiksha Raj, Min Xu, Jimei Yang, and Chun-Hao Paul Huang. Synergistic global-space camera and human reconstruction from videos. In *Proceedings of the IEEE/CVF Conference on Computer Vision and Pattern Recognition*, pages 1216–1226, 2024. 3
- [62] Shunyuan Zheng, Boyao Zhou, Ruizhi Shao, Boning Liu, Shengping Zhang, Liqiang Nie, and Yebin Liu. Gps-gaussian: Generalizable pixel-wise 3d gaussian splatting for real-time human novel view synthesis. In *Proceedings of the IEEE/CVF Conference on Computer Vision and Pattern Recognition*, pages 19680–19690, 2024. 2
- [63] Shenhao Zhu, Junming Leo Chen, Zuozhuo Dai, Yinghui Xu, Xun Cao, Yao Yao, Hao Zhu, and Siyu Zhu. Champ: Controllable and consistent human image animation with 3d parametric guidance. In *European Conference on Computer Vision (ECCV)*, 2024. 1, 3, 4, 5, 7, 12, 13, 14, 15
- [64] Yiyu Zhuang, Jiayi Lv, Hao Wen, Qing Shuai, Ailing Zeng, Hao Zhu, Shifeng Chen, Yujiu Yang, Xun Cao, and Wei Liu. Idol: Instant photorealistic 3d human creation from a single image. *arXiv preprint arXiv:2412.14963*, 2024. 2

GAS: Generative Avatar Synthesis from a Single Image

Supplementary Material

A Limitations and future works

Although our method achieves state-of-the-art performance in both novel view and pose synthesis, it is not free from limitations. (1) Due to the constraints of current off-the-shelf single-image human mesh recovery methods, we use SMPL [30] to establish geometry and appearance conditions for scalable training. However, SMPL lacks expressiveness in regions such as the face and hands, resulting in artifacts in these areas. Future works could explore scalable solutions inspired by recent efforts, such as regional supervision [51, 58]. (2) While we utilize Stable Video Diffusion (SVD) [2] to model view and pose synthesis, achieving strong consistency across both spatial and temporal dimensions, some challenges remain. Specifically, we occasionally observe degraded frame quality and difficulties in accurately generating complex clothing textures, particularly during significant clothing deformations. Addressing the former may involve exploring advanced video generative models, such as Diffusion Transformers [33, 53]. For the latter, leveraging synthetic human datasets with intricate textures presents an exciting avenue for future research.

B Ethical considerations

Human subjects data. We adhere to strict ethical guidelines in the collection and use of data involving human subjects. Below, we provide details on how we obtained each dataset utilized in our work:

- THuman2.1 [55] is a publicly available dataset. We signed the necessary agreement with the dataset authors to obtain access via an official download link.
- 2K2K [13] and MVHumanNet [50] follow the same procedure as THuman2.1, involving an agreement with the authors to obtain official download links.
- TikTok Dataset [19] is publicly available and was downloaded in its preprocessed form from MagicPose [6].
- Additional Real-World Data was manually selected and filtered from the publicly released portions of Champ [63] training data.

Broader Impact. Our proposed method enables affordable and accessible solutions for a wide range of applications. By leveraging generative AI, we transform content generation, making it possible to generate novel views and poses from just a casually-captured single image. It has the potential to revolutionize fields such as virtual reality, gaming, and digital content creation by significantly lowering the barriers to high-quality multi-view synthesis and animation.

However, along with these benefits come potential risks that warrant careful consideration. The misuse of generative AI in creating synthetic content raises ethical concerns, such as the possibility of producing misleading or harmful media. Additionally, privacy concerns may arise when real-world data is used for training, especially when the data involves human subjects. Ensuring robust safeguards, transparent practices, and compliance with ethical standards is crucial to mitigate these risks while maximizing the positive impact of our method.

C Implementation details

C.1 Model architecture

We detail the processing of each conditioning input and their integration into the video diffusion model, as illustrated in Figure 10. Starting with a single reference image $I_{ref} \in \mathbb{R}^{H \times W \times C}$, we extract its VAE latent representation, repeat it T times, and concatenate it with the input noise latent along the channel dimension. This combined representation is passed through a convolutional layer to generate $C_{vae} \in \mathbb{R}^{T \times H_1 \times W_1 \times C_1}$.

For the geometry cue, represented as a sequence of SMPL [30] normal maps, we use a 2D ConvNet ϵ_{geo} to extract features $C_{smpl} \in \mathbb{R}^{T \times H_1 \times W_1 \times C_1}$. Similarly, for the appearance cue, which consists of corresponding NeRF renderings, we pass the sequence through a VAE and subsequently a 2D ConvNet ϵ_{appr} to obtain features $C_{nerf} \in \mathbb{R}^{T \times H_1 \times W_1 \times C_1}$.

The feature representations C_{vae} , C_{smpl} , and C_{nerf} are element-wise added and fed into the diffusion UNet \mathcal{U}_Θ to predict noise. Additionally, the CLIP embedding of the reference image, $h_{clip} \in \mathbb{R}^d$, is repeated T times to match the frame sequence and injected into \mathcal{U}_Θ via cross-attention.

Finally, the switcher, represented as a one-hot vector, is embedded and element-wise added to the time embedding. This is also repeated T times to align with the frame sequence and injected into \mathcal{U}_Θ within the ResNet layers.

C.2 Training details

We leverage a combination of 3D human scans, multi-view videos and monocular videos to train our diffusion UNet \mathcal{U}_Θ , geometry cue encoder ϵ_{geo} and appearance cue encoder ϵ_{appr} .

For 3D scans, we utilize 20 renderings for training the novel view synthesis task. A view is randomly selected as the reference, and the model is tasked with predicting all 20 consecutive novel views. Note that the reference view and the predicted starting view do not need to be the same.

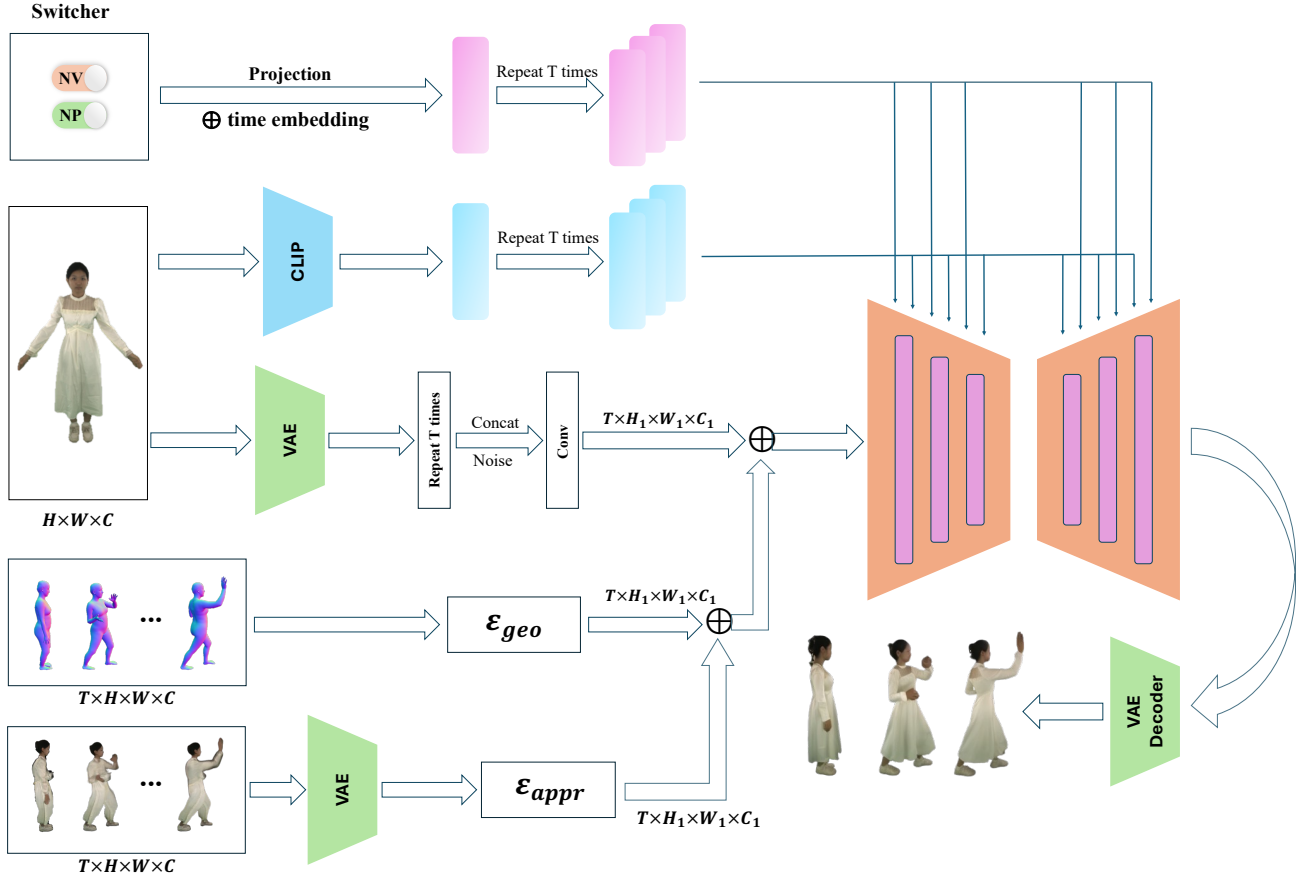


Figure 10. **Network architecture for processing the conditions of the video diffusion model.** ϵ_{geo} and ϵ_{appr} denote geometry encoder and appearance encoder, respectively. \oplus denotes element-wise addition. The switcher embedding and time embedding are injected into the diffusion model in the ResNet layers; the CLIP embedding is injected through the cross attention mechanism.

Furthermore, the order of the predicted views is randomly determined, *i.e.*, either clockwise or counterclockwise.

For multi-view videos, we train the model for the novel pose synthesis task. A frame is randomly selected as the reference image, and the model is tasked with predicting a 20-frame video clip. For a single pose, we also experiment with the novel view synthesis task. However, due to the fluctuating camera trajectory and sparse camera setup, we observe suboptimal outcomes.

For monocular videos, each video is split into a sequence of images at 30 frames per second. We sample one image every four consecutive frames for training. Similarly, a frame is randomly chosen as the reference, and the model is tasked with predicting 20 consecutive frames.

D Additional results

D.1 Video results

We provide additional video results, including in-the-wild avatar synthesis, comparison with baselines, ablations and

additional results. Details explained below:

- **In-the-wild avatar synthesis:** We demonstrate novel view synthesis, pose animation and interactive 4D synthesis on in-the-wild avatars.
- **Comparison with baselines:** We compare our results with Animate Anyone [16] and Champ [63] on THuman [55] for novel view synthesis and TikTok [19] for pose animation. The video results demonstrate our method outperforms the two baseline methods in terms of consistency and quality.
- **Ablations:** We highlight the importance of the dense appearance cue and switcher through the ablation videos.
- **Additional results:** We show novel view synthesis results on MVHumanNet [50]. We also show free-view animation results, where the human subject and the camera are both moving.

D.2 Runtime at inference

Given a single in-the-wild image, we report the runtime of our proposed method, in terms of both novel view and pose

synthesis. The detailed runtime breakdown is as follows. (1) geometry cue rendering; (2) appearance cue rendering; (3) video diffusion inference. The runtime is reported on a single NVIDIA A800 GPU and measured in seconds.

Novel view synthesis. We report the runtime for generating 20 novel views given a single input image, as shown in Table 4.

	20 frames	Per frame
Geo. cue rendering	5.81	0.29
Appr. cue rendering	28.6	1.43
Diffusion inference	15.88	0.79
Total runtime	50.29	2.51

Table 4. **Runtime at inference for generating 20 novel views of a single human image.**

Novel pose synthesis. We report the runtime for generating 100 consecutive novel poses from a single input image, as shown in Table 5. The additional video diffusion inference time arises due to the 6-frame overlap between consecutive video segment windows [41, 58].

	100 frames	Per frame
Geo. cue rendering	29	0.29
Appr. cue rendering	143	1.43
Diffusion inference	106.49	1.06
Total runtime	278.49	2.78

Table 5. **Runtime at inference for generating 50 consecutive novel poses from a single human image.**

Efficiency comparison. We provide a comparison of runtime and VRAM usage with the strongest baseline Champ [63], as shown in Table 6.

	fps	VRAM (GB)
Champ	0.57	9.88
Ours	0.40	5.32

Table 6. **Efficiency comparison with baseline method.**

D.3 Ablation on geometry & appearance cues

We provide a complete quantitative ablation study on the geometry and appearance cue, as shown in Table 10. We use THuman [55] to evaluate the multi-view synthesis and MVHumanNet [50] to evaluate the novel view animation performance.

D.4 Ablation on merging novel view & pose tasks

We provide ablation analysis on merging both novel view and novel pose tasks into one model. From the static novel view synthesis perspective, the unified framework allow us to train on the abundant internet videos - which leads to the improved generalizability, as shown in Figure 8. It does not

hurt the in-domain dataset performance according to Table 9.

From the pose animation perspective, training on additional 3D datasets can improve the quality when we animate the avatar from a novel view, as shown in Table 7.

Training data	PSNR \uparrow	SSIM \uparrow	LPIPS \downarrow	FVD \downarrow
Monocular videos	28.67	0.946	0.041	208.3
Full	28.74	0.945	0.040	188.5

Table 7. **Quantitative ablation on merging view synthesis and pose animation into one model.** Results reported for novel view animation task on MVHumanNet dataset.

D.5 Ablation on switcher

In addition to the qualitative ablation for the switcher presented in the main paper and video results, we also conduct quantitative ablation analysis on the switcher. With the switcher, our method effectively supports both novel view and pose synthesis, while also providing comparable or even better quantitative results, as shown in Table 8.

	PSNR \uparrow	SSIM \uparrow	LPIPS \downarrow	FVD \downarrow
w.o. switcher	26.58	0.944	0.042	198.9
w. switcher	26.77	0.943	0.041	194.8

Table 8. **Ablation on switcher for novel view synthesis task on THuman.**

D.6 Novel pose synthesis on scan datasets

We show the novel pose animation results for subjects in THuman and 2K2K in Figure 11, where the reference images are animated through pose sequences derived from disparate videos.

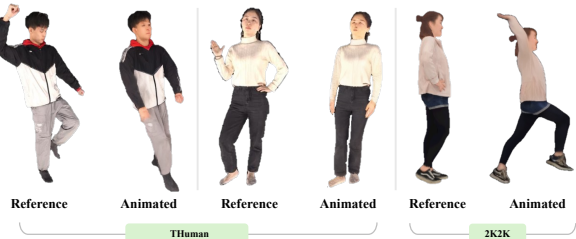


Figure 11. **Novel pose results on THuman and 2K2K.** The reference images are animated by pose sequences derived from MVHumanNet dataset.

D.7 Robustness to input view angles

We train our model using an arbitrary view as input. Thus, we are interested in the novel view synthesis robustness from different input view angles. To this end, we present our quantitative results in Table 11. We find that our pipeline

Training data	PSNR \uparrow		SSIM \uparrow		LPIPS \downarrow		FVD \downarrow	
	THuman	2K2K	THuman	2K2K	THuman	2K2K	THuman	2K2K
3D scans only	26.82	28.76	0.936	0.953	0.040	0.040	189.5	187.9
3D scans+dynamic videos	26.77	28.82	0.943	0.954	0.041	0.039	194.8	191.3

Table 9. **Quantitative ablation on merging view synthesis and pose animation into one model.** Results reported for novel view synthesis task on in-domain THuman and 2K2K testset.

Method	PSNR \uparrow		SSIM \uparrow		LPIPS \downarrow		FVD \downarrow	
	THuman	MVHumanNet	THuman	MVHumanNet	THuman	MVHumanNet	THuman	MVHumanNet
w.o. geo. cue	26.07	28.33	0.938	0.943	0.045	0.044	227.1	210.6
w.o. appear. cue	26.38	27.66	0.938	0.941	0.041	0.043	207.5	234.6
Ours	26.77	28.74	0.943	0.945	0.041	0.040	194.8	188.5

Table 10. **Quantitative ablation on geometry and appearance cues.**

demonstrates robustness with different views of input. Visualized results are shown in Figure 14, where our proposed method can maintain the faithful appearance near the reference view and generate reasonable appearances in unseen regions.

Angle	PSNR \uparrow	SSIM \uparrow	LPIPS \downarrow	FVD \downarrow
Front	28.46	0.952	0.04	178.3
Back	28.34	0.952	0.04	211.5
Left side	29.18	0.956	0.039	199.9
Right side	29.29	0.955	0.038	175.2
Mean	28.82	0.954	0.039	191.3
Std	0.487	0.002	0.001	17.42

Table 11. **Quantitative results on 2K2K dataset for novel view synthesis from different input view angles.**

E Verification of design choices

We found that generative human novel view synthesis remains relatively under-explored, primarily due to the challenge of synthesizing consistent appearances across multiple novel views, especially in unseen regions. We have shown the importance of generalizable appearance cue and geometry cue in the main paper. Here, we aim to additionally validate the choice of leveraging video diffusion models and training with smooth camera orbits.

E.1 Image v.s. video diffusion model

Image diffusion model is believed to be good at image-to-image translation tasks. Specifically, given a single reference image and the target appearance cue, we can train an image diffusion model to synthesize the target image. The model architecture can be a variant of Animate Anyone [16] and Champ [63], where we adopt two ReferenceNets to inject the rich information from the reference image and appearance cue respectively. The results are shown in Figure

12. To enable multi-view consistent synthesis for a single subject, we have tried adding an 1D temporal-axis attention layers [12] and only fine-tune these new added layers. We have also attempted to leverage human geometric prior to construct 3D correspondence across different views [18, 32].

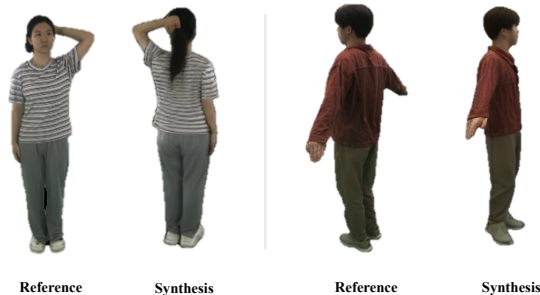


Figure 12. **Image-to-image novel view synthesis on MVHumanNet [50] dataset by using image diffusion model and appearance cue.**

Consistency comparisons. Compared to directly using a pretrained video diffusion model, these image-based diffusion methods exhibit significantly inferior performance. Their results are shown in Figure 13.

Free-view interpolation. Due to GPU memory limitations, we are restricted to training with approximately 20 novel views per subject per batch. During inference, we also test and compare the ability of both models to generate a dense trajectory of novel views (*e.g.*, 100 views). However, neither approach achieves satisfactory results: image-based diffusion models show significant inconsistencies, while video diffusion models produce blurry frames.

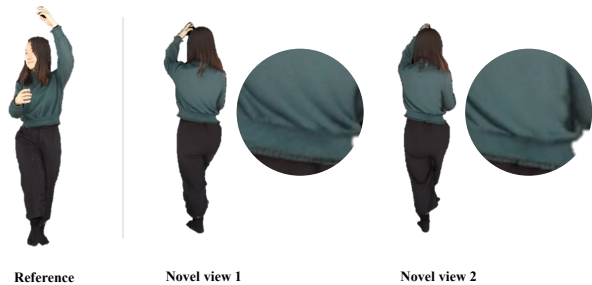
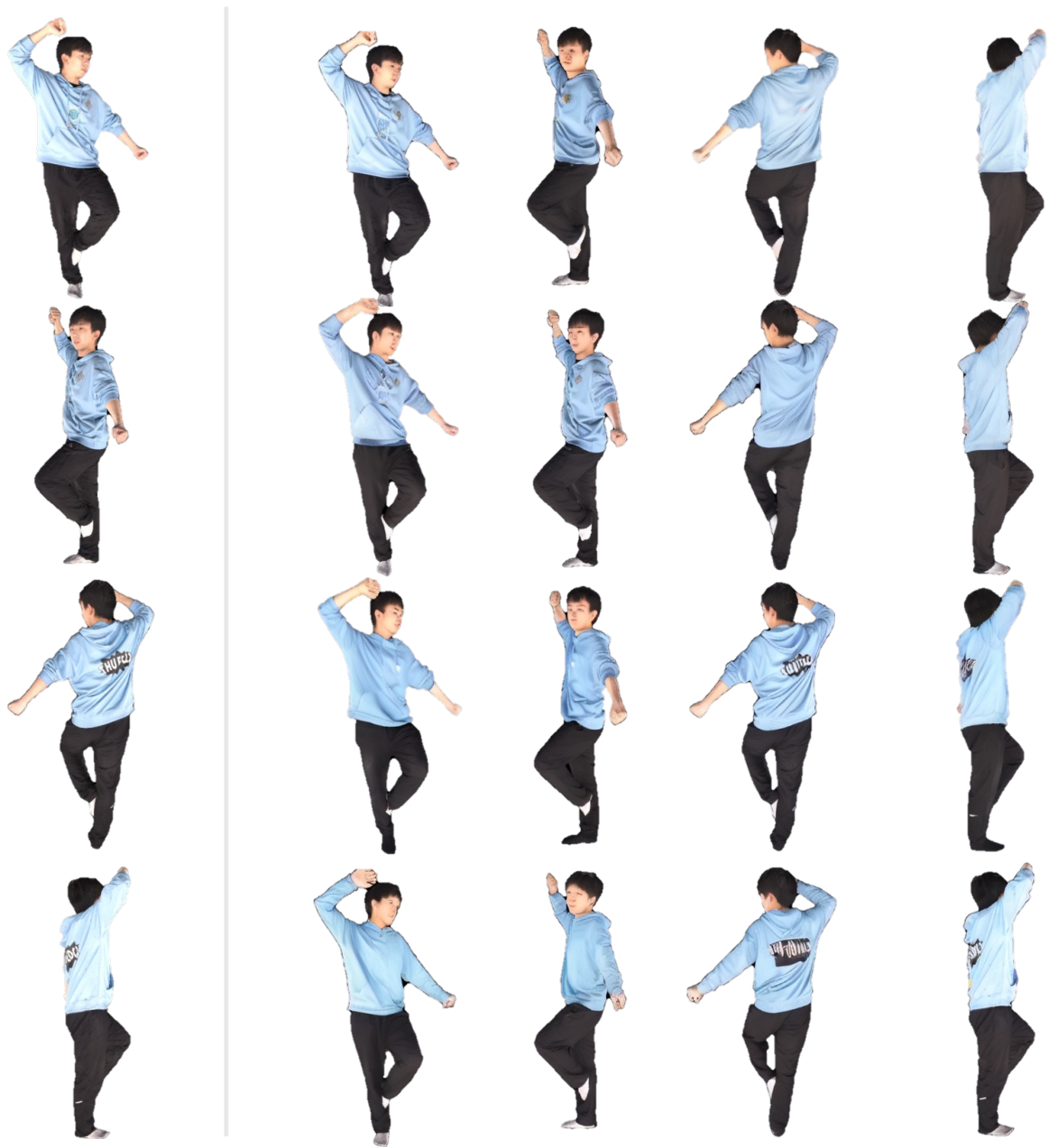


Figure 13. **Novel view synthesis on THuman2.1 by a multi-view image-based diffusion model.** Inconsistent clothing wrinkles appear between two adjacent novel view generations.

E.2 Novel view camera trajectories

On our 3D scan dataset, we render a smooth camera trajectory with the same elevation and evenly distributed azimuth. We also explore the possibility of leveraging the fluctuant novel views in MVHumanNet dataset [50] to learn the multi-view consistency. However, we empirically find that the diffusion models are not able to capture the consistency even with the aid of appearance cues, causing the textures to ‘flow’ across views. The reason might be two folds: 1) number of cameras is too sparse in our adopted subset of MVHumanNet dataset; 2) diffusion models cannot establish accurate correspondence for arbitrary two views with human geometric prior.



Reference

Novel views

Figure 14. Qualitative results of the generated novel views for various input views of the same human subject.